

International Journal of Radiation Biology

ISSN: (Print) (Online) Journal homepage: www.tandfonline.com/journals/irab20

Numerical dosimetry of specific absorption rate of insects exposed to far-field radiofrequency electromagnetic fields

Vera Jeladze, Tamar Nozadze, Besarion Partsvania, Arno Thielens, Levan Shoshiashvili & Teimuraz Gogoladze

To cite this article: Vera Jeladze, Tamar Nozadze, Besarion Partsvania, Arno Thielens, Levan Shoshiashvili & Teimuraz Gogoladze (02 Jan 2025): Numerical dosimetry of specific absorption rate of insects exposed to far-field radiofrequency electromagnetic fields, International Journal of Radiation Biology, DOI: 10.1080/09553002.2024.2442693

To link to this article: https://doi.org/10.1080/09553002.2024.2442693

Published online: 02 Jan 2025.

Submit your article to this journal

Article views: 9

View related articles

View Crossmark data

Full Terms & Conditions of access and use can be found at
https://www.tandfonline.com/action/journalInformation?journalCode=irab20

INTERNATIONAL JOURNAL OF RADIATION BIOLOGY
https://doi.org/10.1080/09553002.2024.2442693

Taylor & Francis
Taylor & Francis Group

ORIGINAL ARTICLE

Check for updates

Numerical dosimetry of specific absorption rate of insects exposed to far-field radiofrequency electromagnetic fields

Vera Jeladze[a,b], Tamar Nozadze[c], Besarion Partsvania[a], Arno Thielens[d], Levan Shoshiashvili[c] and Teimuraz Gogoladze[a]

[a]Department of Biocybernetics, Vladimer Chavchanidze Institute of Cybernetics of the Georgian Technical University, Tbilisi, Georgia; [b]Department of Information Technology, Georgian National University SEU, Tbilisi, Georgia; [c]Department of Electrical and Electronics Engineering, Ivane Javakhishvili Tbilisi State University, Tbilisi, Georgia; [d]Photonics Initiative, ASRC, The Graduate Center of the City University of New York, New York, New York, USA

ABSTRACT

Purpose: This paper reports a study of electromagnetic field (EMF) exposure of several adult insects: a ladybug, a honey bee worker, a wasp, and a mantis at frequencies ranging from 2.5 to 100 GHz. The purpose was to estimate the specific absorption rate (SAR) in insect tissues, including the brain, in order to predict the possible biological effects caused by EMF energy absorption.

Method: Numerical dosimetry was executed using the finite-difference time-domain (FDTD) method. Insects were modeled as 3-tissue heterogeneous dielectric objects, including the cuticle, the inner tissue, and the brain tissue. The EMF source was modeled as sinusoidal plane waves at a single frequency (far-field exposure).

Results: The whole-body averaged, tissue averaged, and 1 milligram SAR values were determined in insects for all considered frequencies for 10 different incident plane waves. SAR values were normalized to the incident power density of 1 mW/cm^2. Maximal EMF absorption in the inner and brain tissues was observed at 6, 12, and 25 GHz for the considered insects, except the brain tissue of a ladybug (max at 60 GHz).

Conclusion: The paper presented the first estimation of the SAR for multiple insects over a wide range of RF frequencies using 3-tissue heterogenous insect 3D models created for this specific research. The selection of tissues' dielectric properties was validated. The obtained results showed that EMF energy absorption in insects highly depends on frequency, polarization, and insect morphology.

ARTICLE HISTORY
Received 4 July 2024
Revised 19 November 2024
Accepted 11 December 2024

KEYWORDS
Radiofrequency; electromagnetic field exposure; mm waves; insect; SAR; FDTD

Introduction

The development of the 5th generation (5 G) and next-generation of wireless communication networks could alter the nature of radio-frequency electromagnetic field (RF-EMF) exposure in the environment. Biological organisms, including insects, are exposed to these fields. A fraction of these RF-EMFs is absorbed by their bodies and can cause dielectric heating (International Commission on Non-Ionizing Radiation Protection 2020). The future planned telecommunication systems (Pi and Khan 2011; Colombi et al. 2015) will use millimeter wavelengths (30–300 GHz), which have wavelengths comparable to the body (part) dimensions of some small-size biological objects, such as insects. This could cause whole-body or partial-body resonance (Hirata et al. 2007) during exposure. For some insects, the resonant frequencies also could be found in the currently used and future planned frequencies between 2–30 GHz. The study of these issues is a significant and relevant topic today as insects, especially bees, pollinate 80% of all plants (Ollerton et al. 2011) and are an essential part of the ecosystem and biodiversity.

Most existing studies (Marec et al. 1985; Wang and Tang 2001; Sanborn 2008; Pall 2013; Cammaerts et al. 2014; Vijver et al. 2014; Balmori 2015; Fauzi and Corebina 2015; Lázaro et al. 2016) mainly focused on determining the mechanisms of bio-effects of RF-EMF exposure up to 6 GHz by laboratory experiments. These studies showed that RF-EMF exposure above some yet to be determined thresholds can affect insect behavior, physiology, morphology, reproduction, orientation, etc. Some studies related to insect RF-EMF exposure used numerical simulations and numerical insect models at frequencies from 0.6 to 300 GHz (Thielens et al. 2018, 2020; De Borre et al. 2021; Herssens et al. 2022; Toribio et al. 2022). According to these studies, most insects show a maximal absorption of RF-EMF at frequencies above 6 GHz. Herssens et al. (2022) also revealed that the absorbed power strongly depends on the volume of insects. In these studies, insects were modeled as homogeneous (single-tissued) objects; in reality, they are heterogeneous biological

CONTACT Vera Jeladze v.jeladze@gtu.ge Department of Biocybernetics, Vladimer Chavchanidze Institute of Cybernetics of the Georgian Technical University, 5 Z. Anjaparidze Str., Tbilisi 0186, Georgia; Department of Information Technologies, Georgian National University SEU, 9 Tsinandali Str., Tbilisi 0144, Georgia.
Copyright © 2024 Taylor & Francis Group LLC.

organisms with different tissue dielectric properties. Because of this mismatch between simulation and reality, it is impossible to understand the biological effects of insect EMF exposure thoroughly. Determining tissue-specific specific absorption rates (SARs) in insects could mean a step forward in our understanding of this topic. However, such has never been determined in existing studies on insects.

Therefore, this research aims to develop heterogeneous insect 3D models and determine the EMF energy absorption in insect tissues quantified by the SAR (specific absorption rate [W/kg]). As a first step toward reaching this goal, this novel research focuses on a honey bee worker (*Apis mellifera*), a wasp (*Vespula vulgaris*), a ladybug (*Coccinella septempunctata*), and a mantis (*Mantis religiosa*), all in adult form, as model organisms. The role of the honeybee as important insect is known to all (Aslan et al. 2016; Papa et al. 2022). The most important ecosystem service provided by wasps is pest control (Prezoto et al. 2019), as wasps hunt live prey like flies, caterpillars, spiders, etc. Mantes eat mainly insects and other small animals, and many gardeners and farmers welcome mantes because the insects they eat are often pests that hurt crops (Schuster and Whicker 1983). Ladybugs prey on crop-damaging aphids, mealybugs, and other destructive insect pests (Dixon 2000). Therefore, all these insects are worth investigating.

Methods

The subject of this paper is to study the absorption of RF-EMF emitted from 5 G and next-generation telecommunication networks from 2.5 to 100 GHz in insects using numerical dosimetry. As insects are complex-shaped and heterogeneous biological objects, we use the most suitable numerical technique: the Finite-Difference Time-Domain (FDTD) method (Taflove and Hagness 2005) for EM simulations to evaluate the absorption of EMF energy quantified by SAR of insect tissues. In particular, we were interested in how this absorption is distributed in an insect's body. This required the development of heterogeneous 3D models of selected insects for EM simulations, which could lead to more accurate results of tissue-specific and whole-body SARs. Because the body dimensions of most insects are in the millimeter and centimeter ranges, our hypothesis was that resonant effects can occur in the studied frequency range. We assumed that RF-EMFs can penetrate their body at certain frequencies and could potentially impact their nervous system. Therefore, the focus was on estimating SAR values inside the brain tissues of insects, as the brain represents the main vital organ. It was previously shown that this absorption depends on insect size (Herssens et al. 2022). Therefore, in the first stage, 4 insects of different sizes were selected for this research.

To achieve the set goals of this research, we took the following steps: (1) the creation and discretization of the insect's 3D realistic heterogeneous model, (2) selecting and assigning dielectric properties to each tissue, and (3) conducting EM simulations using the FDTD technique to evaluate the absorption of EMF energy (expressed in SAR) inside the insect's body tissues. In the research, we used the FDTD-based EM and Thermal solver FDTD Lab (Tbilisi State University, Tbilisi, Georgia) for EM simulations. In FDTD Lab, as in other FDTD-based programs, the EM solver is based on the numerical solution of the Maxwell differential Equations by the FDTD method and Yee Algorithm (Yee 1966; Taflove and Hagness 2005); FDTD Lab also has a SAR average that allows SAR values to be averaged over a volume of any tissue mass. SAR in humans is usually averaged over a standardized tissue volume, typically 1 g or 10 g. Such an average is impossible for insects because of their small mass (close to 1 g). Therefore, we chose to estimate 1 mg-averaged SAR values in insect tissues to visualize the SAR distribution within the insects. In humans, 1 or 10 g-averaged SAR is used as a proxy for tissue heating. In insects, it is currently unknown what averaging volume is the best representation of tissue heating. We nonetheless decided to proceed with 1 mg averaging in order to represent SAR, because SAR is meaningless without an averaging volume. We also evaluated the maximal 1 mg SAR value in the whole insect and each separate tissue denoted the peak 1 mg SAR throughout this paper. In a second step, we averaged the SAR over each separate tissue of the insect models and the whole body by dividing the total absorbed power in individual tissues or the whole body by the mass of these tissues or the whole body, respectively.

Insect models and tissue parameters

The selected insects are modeled as heterogeneous dielectric objects using 3 different tissues: the cuticle, the inner tissue (inside the cuticle), and the brain.

For the creation of such heterogeneous insect models, the insect bodies and body parts (see Figures 1 and 2) were processed in Stereolithography (STL) format using graphics software: Blender (Stichting Blender Foundation, Amsterdam, Netherlands) and Netfabb Premium (Autodesk, San Francisco, USA).

The initial insect models were taken from open repositories of 3D models (Open3DModel 2024; CadNav 3D 2024). These were then adapted using the following steps. First, the original models were smoothed by bulging areas on the torso, head, and abdomen. Second, a brain model was inserted into the homogeneous models. The honeybee and wasp brain models (Figure 2(a)) were created using Blender based on the brain model of Heinze et al. (2021). The mantis brain model (Figure 2(b)) was based on the brain model from Rosner et al. (2017) and also created in Blender by converting 2D images into 3D. The Ladybug brain is much smaller than the brains of the other insects studied and we did not find any available models for this brain. Therefore, we modeled it as a spheroid (Figure 2(c)). The dimensions (Length, Width, Height) of the insect and brain models are presented in Table 1.

Third, inner tissues (excluding brain) were defined in the insect models of insects by cutting the limbs and extruding a layer of 0.2 mm inside the primary models, see Figure 3 for an illustration.

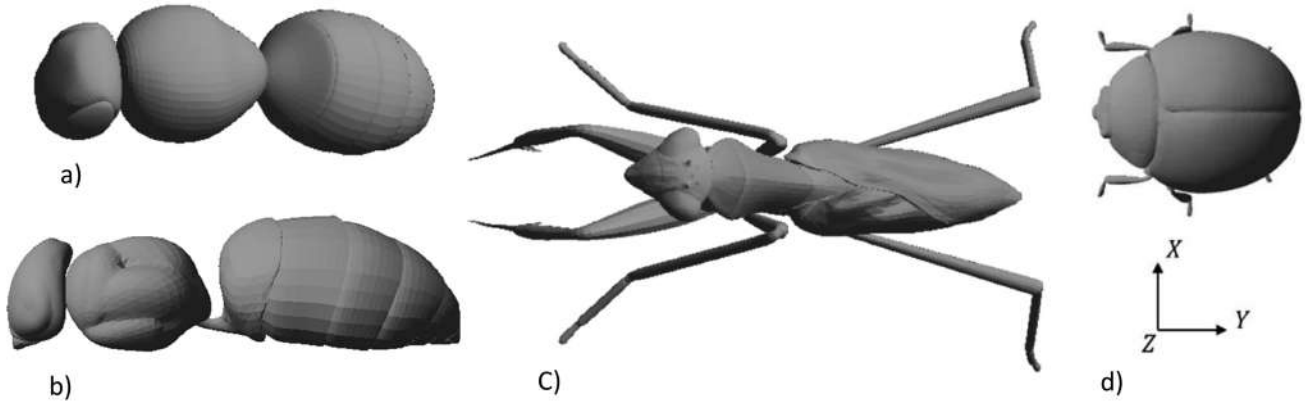


Figure 1. Insects' 3D models in STL format: (a) the honeybee, (b) the wasp, (c) the mantis, and (d) the ladybug. The length of all insects is oriented along the Y-axis, the width—along the X-axis, and the height—along the Z-axis.

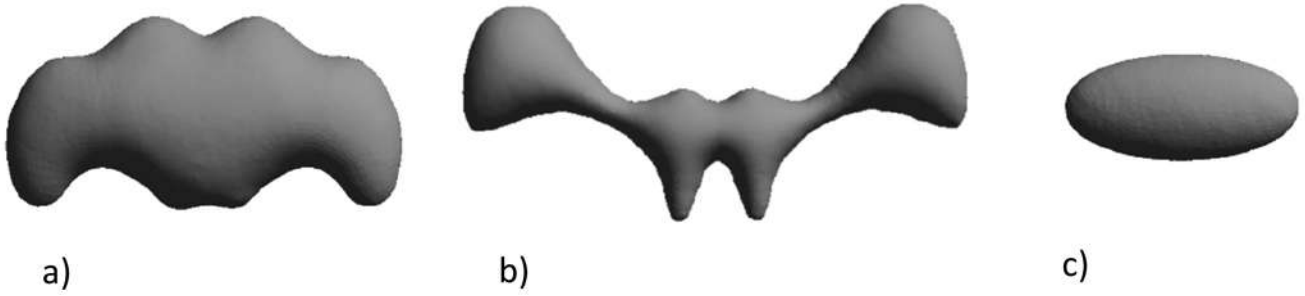


Figure 2. Brain models for (a) the honeybee and the wasp, (b) the mantis, and (c) the ladybug.

Table 1. Dimensions of the insect models and their brain models.

Insects	Length (mm)	Width (mm)	Height (mm)	Volume (mm^3)	Mass (mg)
Ladybug	7.2	5.4	3.6	33.71	36.20
Honey bee	13.4	5.0	5.2	122.19	131.24
Wasp	17.4	5.4	6.0	146.28	156.82
Mantis	68.3	13.7	24.6	2097.44	2252.65
Ladybug brain	1	0.4	0.4	0.105	0.11
Honeybee brain	1.8	0.8	1.3	0.931	0.97
Wasp brain	2	1	1.5	1.035	1.08
Mantis brain	3.7	1.1	1.6	1.371	1.43

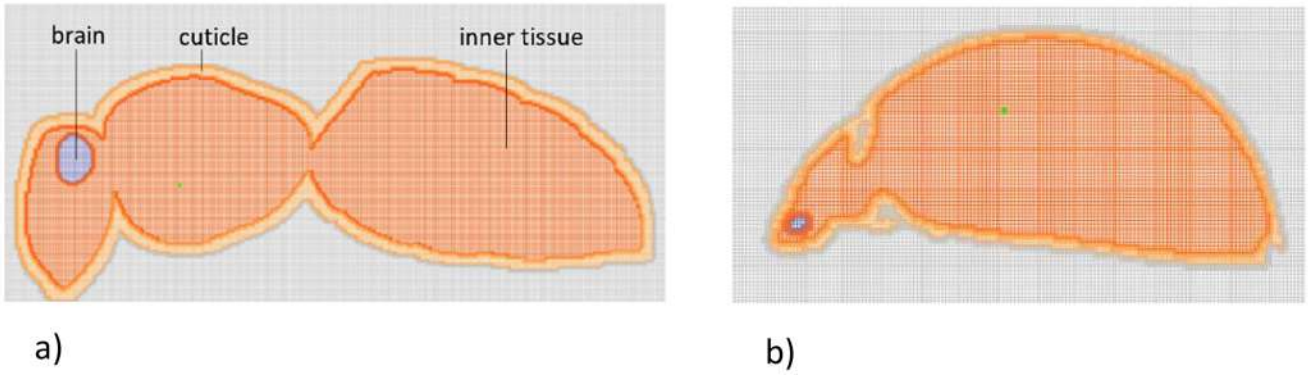


Figure 3. Mid-sagittal cross-sections of two 3-tissue discrete heterogeneous models of: (a) the honeybee and (b) the ladybug.

Tissue-specific dielectric properties of insects are rare and do not exist for the selected insects for our current studies. Therefore, we decided to use the IT'IS Database of tissue properties (Hasgall et al. 2022), which provides frequency-dependent EM parameters (permittivity and conductivity) for many biological tissues from 10 Hz to 100 GHz.

The cuticle of insects was modeled as cartilage tissue. This choice is based on the observation that the EM

properties (permittivity and conductivity) of cartilage from the IT'IS database are very close to the EM properties of the insects in previous studies (Thielens et al. 2018, 2020). The permittivity and conductivity of inner tissue were obtained by averaging these parameters of the following internal tissues from the IT'IS database: muscle, heart muscle, stomach, stomach lumen, small and large intestines, gland, and nerve. The brain EM parameters are the average values of brain white and grey matter parameters. The density of the cuticle is the density value of the cartilage tissue and the density values of brain and inner tissues of selected insects were determined using the same methods as the permittivity and conductivity from the IT'IS database. The obtained values of tissue parameters are given in Table 2.

The validity of this novel approach for selecting tissue parameters of insects was initially checked for a 3-tissued sphere with a 5 mm radius (see Figure 4). The outer layer has 0.2 mm thickness and represents cuticle tissue; the inner tissue is created using a sphere with a 4.8 mm radius; the brain tissue is created using a smaller sphere (radius = 1 mm) whose center has an offset of 3.5 mm from the main center. This sphere was exposed to incident plane waves at 2, 3, 6, 12, 25, and 60 GHz frequencies. The EMF exposure configuration is shown in Figure 4. The validation results are presented in the Results section under the heading 'Validation of the Results'.

EMF exposure modeling

In this research, the EMF source was modeled as sinusoidal plane waves at a single frequency (far-field exposure). For each selected harmonic frequency (9 harmonic frequencies: 2.5, 3.7, 6, 12, 25, 40, 60, 85, and100 GHz), 10 incident plane waves fall on the insect models from five directions (front, back, top, bottom, and left) defined by the Cartesian coordinate system. Two orthogonal, incident E-field polarizations are chosen for each direction. These incident E-fields are presented in Figure 5. We did not consider the right side direction of incidence because it gives the same result as the left incidence direction, as the insect models have symmetry relative to the YZ plane.

The next step was to determine the discretization size of the simulation domain and create a 3-dimensional grid for FDTD modeling. The grid element (voxel) is a cube. For selecting grid discretization size, we took into account its dependence on the wavelength, the object (insect) size and tissue properties, and the desired spatial accuracy according to the FDTD method. To get a stable solution (Hand 2008), the grid step (Δ) needs to fulfill $\Delta < \lambda_0 / \sqrt{|\epsilon_r^*|}$, where $\lambda_0 = c / f$ and $|\epsilon_r^*| = \sqrt{(\epsilon_r')^2 + (\sigma / (2\pi f \epsilon_0))^2}$, when we consider dielectric tissues (complex media) in the simulation domain. Taking into account these requirements, the voxel size (grid discretization size) equals 0.05 mm (50 µm) for a ladybug and honeybee and 0.1 mm (100 µm) for a wasp and mantis along the all-axis in each calculation.

The next stage of this study was to conduct numerical simulations using FDTD Lab to estimate SAR values in the body tissues of selected insects.

Results

In the frame of this research, 3-tissue heterogeneous 3D models of a honeybee, a wasp, a ladybug, and a mantis were created with averaged EM parameters (Figures 1–3, Table 2).

For each insect, we have conducted 90 EM simulations (10 directions of the incident plane wave for 9 frequencies). In this research, all SAR values are given in units of W/kg and are normalized to the incident power density of 1 mW/cm^2. The obtained results are presented below.

RF-EMF absorption in the ladybug

First of all, we show results for the ladybug, as it is the smallest insect in our study. Figure 6 shows peak 1 mg SAR values inside the ladybug's whole body for all frequencies and E-field polarizations. Peak 1 mg SAR values depend on polarization and significantly increase from 12 GHz to 100 GHz. They are in the range of 1–10 W/kg for 2.5, 3.7, and 6 GHz frequencies and increase up to 10–50 W/kg from 12 GHz to 100 GHz. Figure 7 shows the 1 mg SAR distribution inside the ladybug when the E-field is directed along the longitudinal axis of the ladybug. The results showed that high EMF absorption is observed inside the head area at 25, 40, 60, 85, and 100 GHz frequencies. The most efficient absorption of RF-EMFs in the inner tissue is found at 12 GHz. Such an absorption happened for all polarization at 12 GHz, as illustrated in Figure 7(b). The half wavelengths in the ladybug tissues at 12 GHz are $\lambda_c(12\,\text{GHz})/2 = 1.90$ mm, $\lambda_i(12\,\text{GHz})/2 = 2.35$ mm, $\lambda_b(12\,\text{GHz})/2 = 2.11$ mm. The dimensions (L × W × H) of the

Table 2. Tissue parameters used in this study.

	Cuticle		inner tissue		brain	
Tissue parameters	ε	σ [S/m]	ε	σ [S/m]	ε	σ [S/m]
2.5 GHz	38.7	1.79	51.5	2.0	42.5	1.54
3.7 GHz	36.2	2.83	49.8	3.0	40.9	2.38
6 GHz	31.8	5.09	47.2	5.5	38.1	4.44
12 GHz	23.2	10.8	38.2	13.9	31.0	11.1
25 GHz	14.3	18.8	25.3	30.1	20.2	23.7
40 GHz	10.3	23.7	17.2	41.8	14.1	32.5
60 GHz	8.04	27.5	12.2	50.7	10.2	39.05
85 GHz	6.75	30.4	9.3	56.9	8.2	43.7
100 GHz	6.30	31.7	8.28	59.49	7.24	45.6
	Density ρ [kg/m^3]					
	1100		1061		1043	

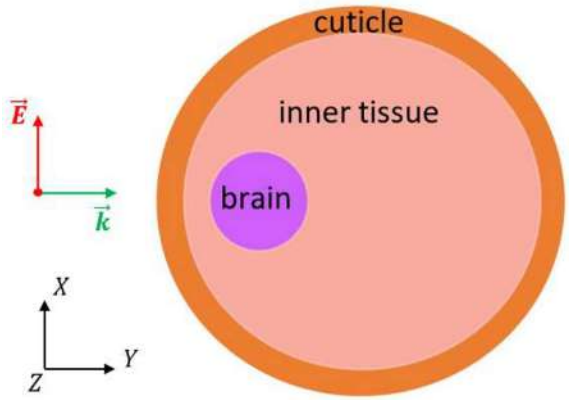


Figure 4. Sphere with 3 tissues (rad = 5 mm).

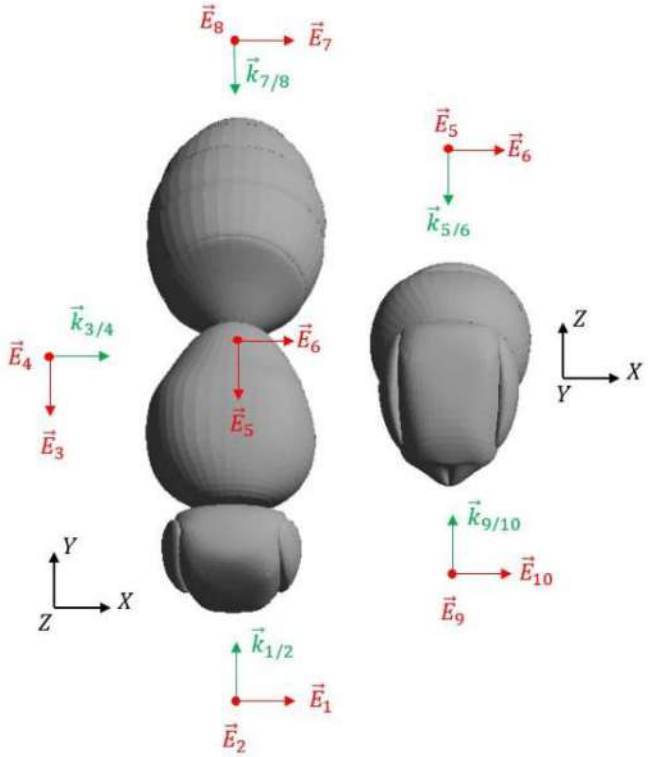


Figure 5. Considered E-field polarizations and incidence directions of plane waves.

ladybug's inner tissue without the head are 5.66 × 4.74 × 2.75 [mm]. The height of the inner tissue 2.75 mm is close to the half wavelength $\lambda_i / 2 = 2.35$ mm at 12 GHz, while the width of the inner tissue 4.74 mm is quite close to the wavelength in the inner tissue $\lambda_i = 4.70$ mm at 12 GHz. Therefore, the resonant absorption of EMFs inside the ladybug body at 12 GHz (Figure 7(b)), can be explained. The hemispherical shape of the ladybug's body also plays a significant role in the efficient absorption of EMFs.

RF-EMF absorption in the honeybee and wasp

Figure 8 shows the peak 1 mg SAR values over the whole body of the honeybee and wasp for each E-field polarization at all considered frequencies. There are large variations in the peak 1 mg SAR values up to 12 GHz. In particular, a sharp increase of SAR could be observed in the cases when the incidence of the plane waves to the insect bodies occurred from the left, top, and bottom directions and the E-fields were directed along the insects' length (pol. E3, E5, E9). These sharply increased SAR peaks are localized in the insects' petioles.

Figure 9 shows 1 mg SAR distributions for the honey bee model in some sections in the case of different E-field polarizations (pol. E4, E5, E6). As can be seen, the EMF penetrates deeper into the honeybee tissues at 6 GHz and 12 GHz. In contrast, at other frequencies, the absorption of EM field energy mainly occurs in the superficial tissues of the honey bee body. Therefore, the SAR peak values are localized in the same areas.

RF-EMF absorption in the mantis

Figure 10 shows peak 1 mg SAR values inside the whole body of the mantis for all frequencies and E-field polarizations. Like other insects, the results show a sharp change of 1 mg SAR in the mantis body depending on frequency and polarization. 1 mg SAR values are higher for frequencies from 12 GHz to 100 GHz than at lower frequencies and range between 10–80 W/kg. 1 mg SAR distributions inside the mantis body for all frequencies are presented in Figure 11 when the E-field vector was directed along the mantis longest dimension. Because the size of the mantis is large compared to the other insects discussed, and the body shape is quite different, here we have a different picture of the SAR distribution. EMF absorption in internal tissue was higher for frequencies of 2.5, 3.7, and 6 GHz, but higher EMF absorption at other frequencies was found in the area of the neck.

Tissue-specific SAR values and comparison of insects

Figure 12 shows the tissue-averaged and WBA SAR values (averaged for 10 polarizations of incident E-field) for all frequencies and for each insect and tissue. Tissue-averaged SAR values inside the brain tissues of the honeybee, wasp, and mantis are much higher at 12, 25 and 40 GHz frequencies and range between 2–6 W/kg. The peak values of brain SAR were observed at 25 GHz for honeybee and mantis; for the wasp, brain SAR is maximal at 12 GHz frequency. SAR values in the brain tissue of the ladybug are much higher compared to the brain SAR values of the other insects studied and range between 5–10 W/kg at 12, 25, 40, 60, 85, and 100 GHz frequencies. This is due to the fact that the size of the ladybug's head and brain are smaller compared to the other insects. The maximal SAR value of 10 W/kg in a ladybug's brain tissue is observed at 60 GHz frequency. Thus, the ladybug has the highest brain SAR compared to others.

The ladybug has the highest WBA SAR of all studied insects from 12 GHz to 100 GHz ranging from 3.9 – 4.5 W/kg and has the lowest WBA SAR of all studied insects. At lower

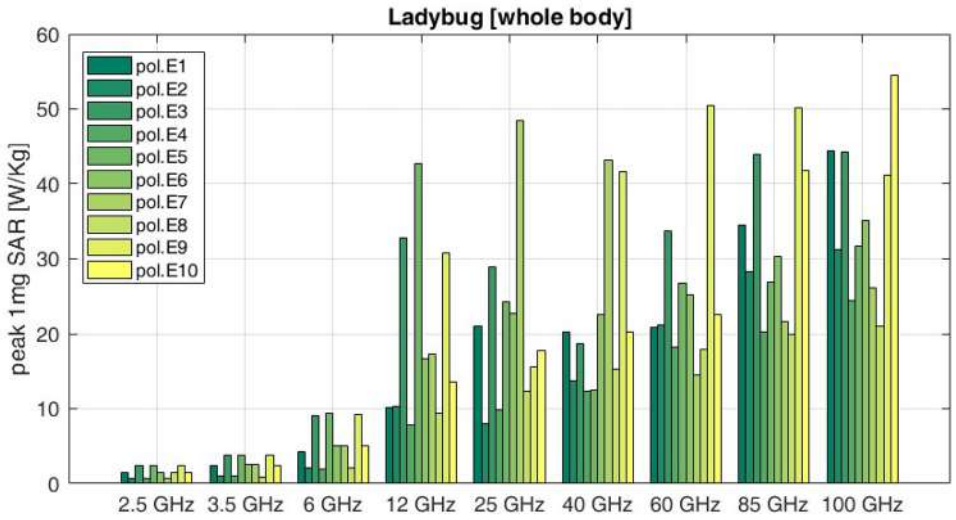


Figure 6. Peak 1 mg SAR values in the ladybugs's whole body for an incident power density of 1 mW/cm^2.

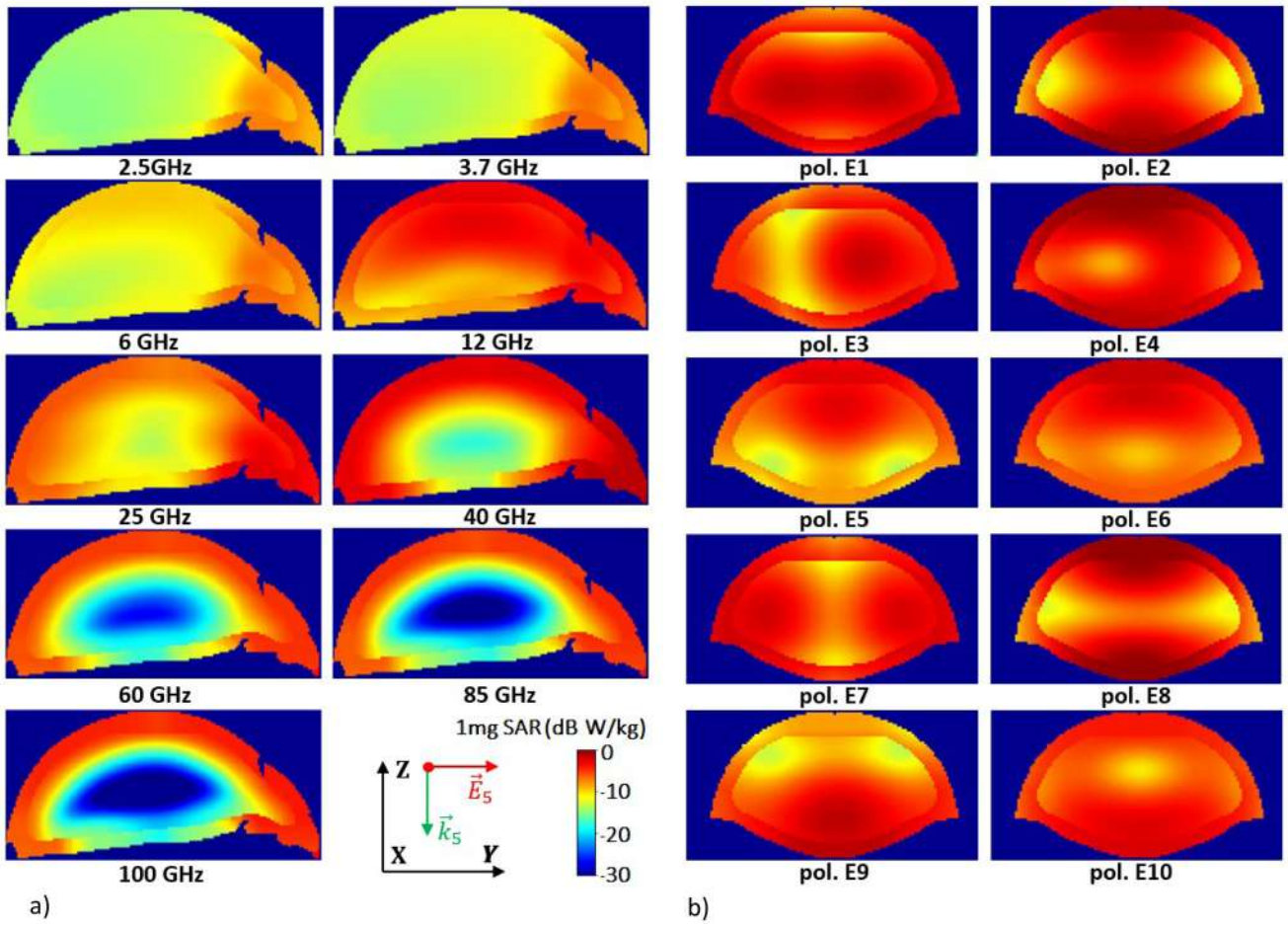


Figure 7. 1 mg SAR distribution inside the ladybug model for (a) the mid-sagittal section of the insect, when the E-vector is directed along the Y-axis (Pol. E5), and (b) for all 10 plane waves at 12 GHz frequency in a section of the ladybug parallel to the ZX plane. 1 mg SAR values on the ruler are given in W/kg using a logarithmic (dB) scale. This ruler also belongs to Figure 9(b).

frequencies (2.5, 3.7, and 6 GHz) the mantis has the highest WBA SAR in the range of 1.8 – 3 W/kg.

The wasp has the highest inner tissue SAR of 5.9 W/kg (12 GHz) compared to other insects. The honeybee and ladybug also have inner tissue peak absorptions at 12 GHz. The inner tissue peak absorption for the mantis is observed at 6 GHz, which can be explained by the fact that the mantis body size is close to the wavelength at 6 GHz. For all studied insects, the inner tissue and whole body SAR curves show very similar trends as a function of frequency and the whole body and inner

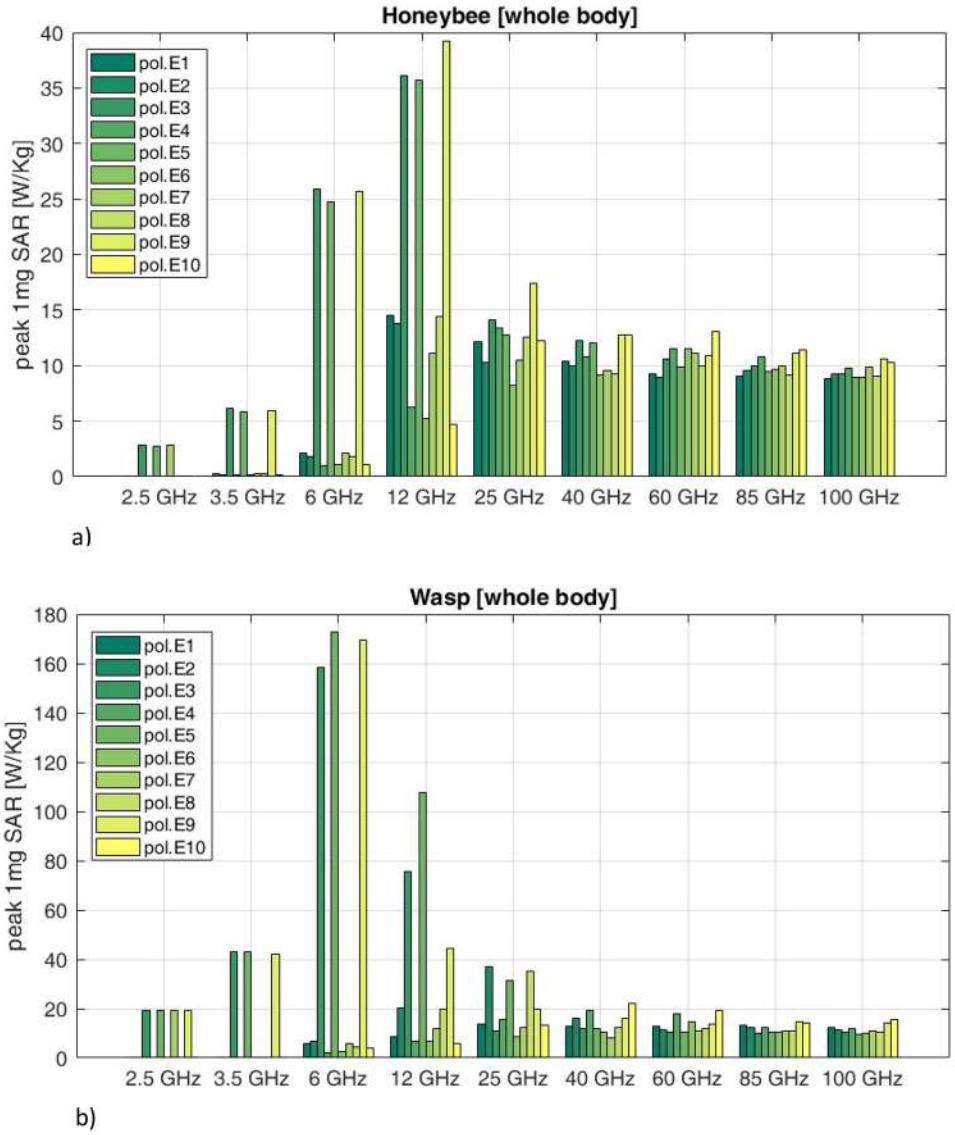


Figure 8. Peak 1 mg SAR values in the (a) honeybee's and (b) wasp's whole body for an incident power density of 1 mW/cm^2.

tissue absorption show peak efficiencies at the same frequencies. The other tissues show distinctly different trends as a function of frequency. This reinforces the importance of using tissue-specific averaging since the whole body averaging is not necessarily a good proxy for the brain or cuticle. This observation is in line with what was found for humans (Liorni et al. 2020).

Validation of the results

To prove the validity of the above-presented results, below are the results that show the validity of the choice of the tissue EM parameters and densities, grid step, and EM simulation software.

Table 3 shows the comparison of the tissue-averaged SAR and WBA SAR values in W/kg for the 3-tissue sphere (Figure 4) that has the tissue EM parameters like insects in our research (based on our novel approach) and for the sphere that has the same parameters for all 3-tissues, which were taken from (Thielens et al. 2018), where the insects are presented as a homogeneous object with a single tissue.

Based on the comparison, we can conclude that the obtained tissue-averaged SAR and WBA SAR values are in good agreement and the relative difference doesn't exceed 17%. Future research should validate tissue-specific insect dielectric properties through measurements. Table 4 compares the tissue-averaged SAR, 1 mg SAR, and WBA SAR values in W/kg for the same 3-tissue sphere at 60 GHz (Figure 4), which were calculated using densities from Table 1 (used in our EM simulations) and density variations. ρ_c = 1100, ρ_i= 1061, ρ_b = 1043 [kg/m^3] represent the densities of the cuticle, inner tissue, and brain. The comparison of the results shows that if we increase each density value by 50, 100, 150, and 200 [kg/m^3], the decrement of the obtained SAR values doesn't exceed 5%, 10%, 15%, and 20%, respectively. If we reduce the densities, we will get a similar trend of increasing SAR values. Based on the observation of the IT'IS database of biological tissue properties, we suppose that the density variations will not be more than ±50 or ±100 [kg/m^3] and the relative differences between the SAR values do not exceed 10%.

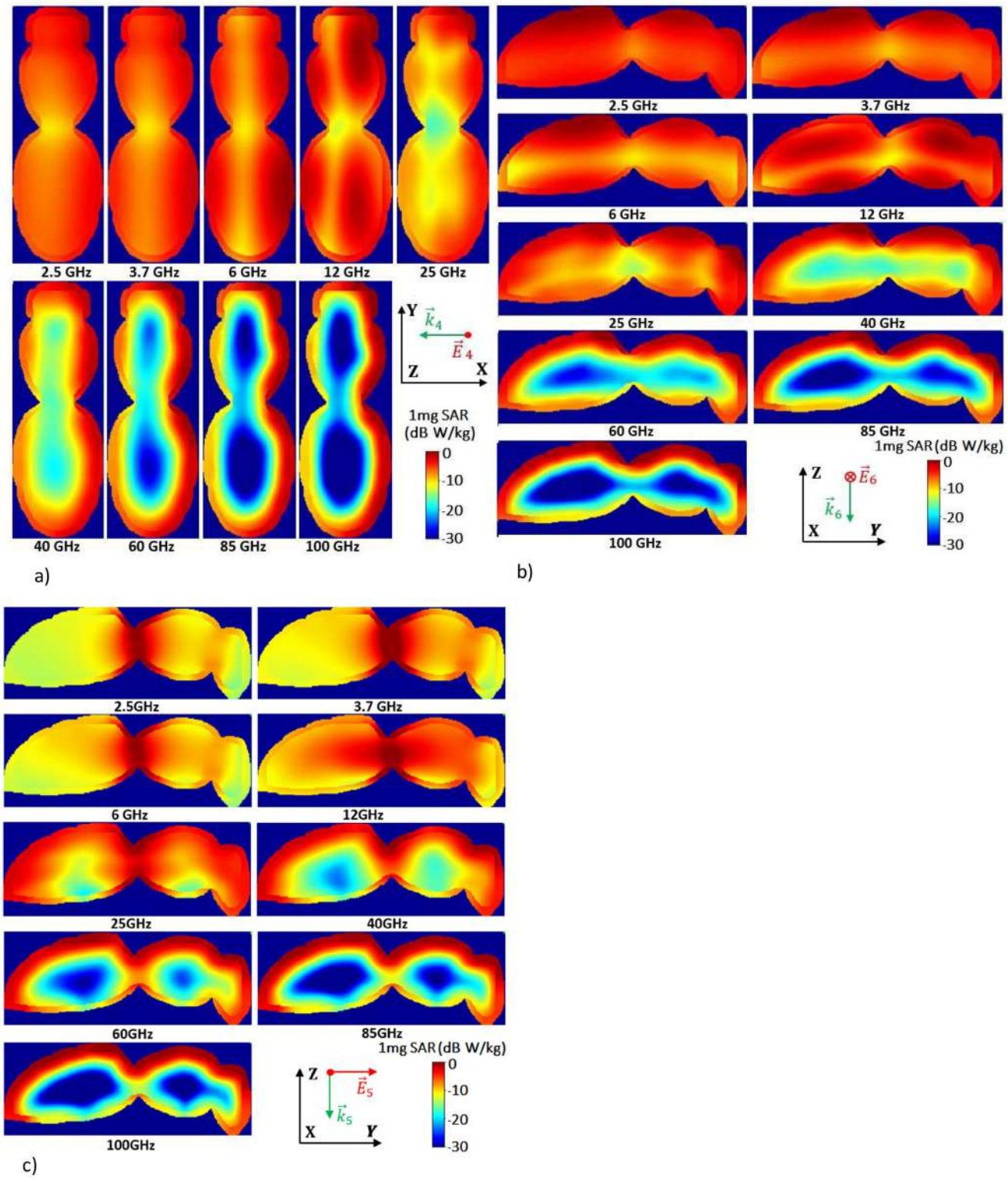


Figure 9. 1 mg SAR distribution inside the honeybee model (a) at the parallel section of the XY plane. The E-vector is directed along the Z-axis (Pol. E4), (b) at the parallel section of the ZY plane. The E-vector is directed along the X-axis (Pol. E6), and (c) at the parallel section of the ZY plane. The E-vector is directed along the Y-axis (Pol. E5). 1 mg SAR values on the ruler are given in W/kg using a logarithmic (dB) scale.

The FDTD technique requires simulation time to be predefined to reach a stable solution, which also depends on the wavelength, the spatial resolution (grid step), and the simulation domain size. The time step satisfies the Courant's condition for 3-dimensional grid $\Delta t \leq \Delta / c\sqrt{3}$ (Taflove and Hagness 2005). We chose grid step (Δ) of 0.05 mm (50 μm) for a ladybug and honeybee and 0.1 mm (100 μm) for wasp and mantis as they have larger body sizes. This allowed us to reduce the simulation time, especially for Mantis. For all considered frequencies (from 2.5 to 100 GHz), both grid steps 50 μm and 100 μm meet the requirements of the FDTD method in the case of EMF exposure on a dielectric object: $\Delta < 0.1\lambda_0 / \sqrt{|\epsilon_r^*|}$.

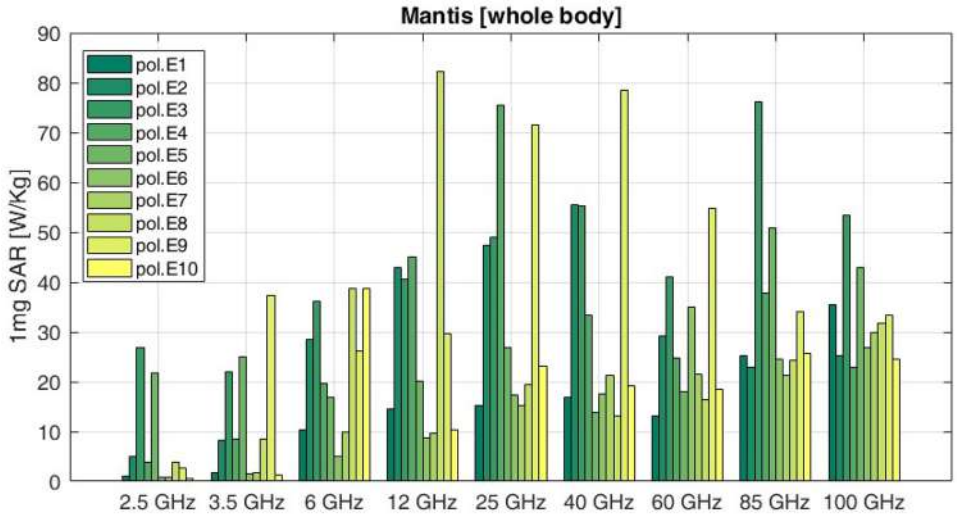


Figure 10. Peak 1 mg SAR values in the mantis for an incident power density of 1 mW/cm^2.

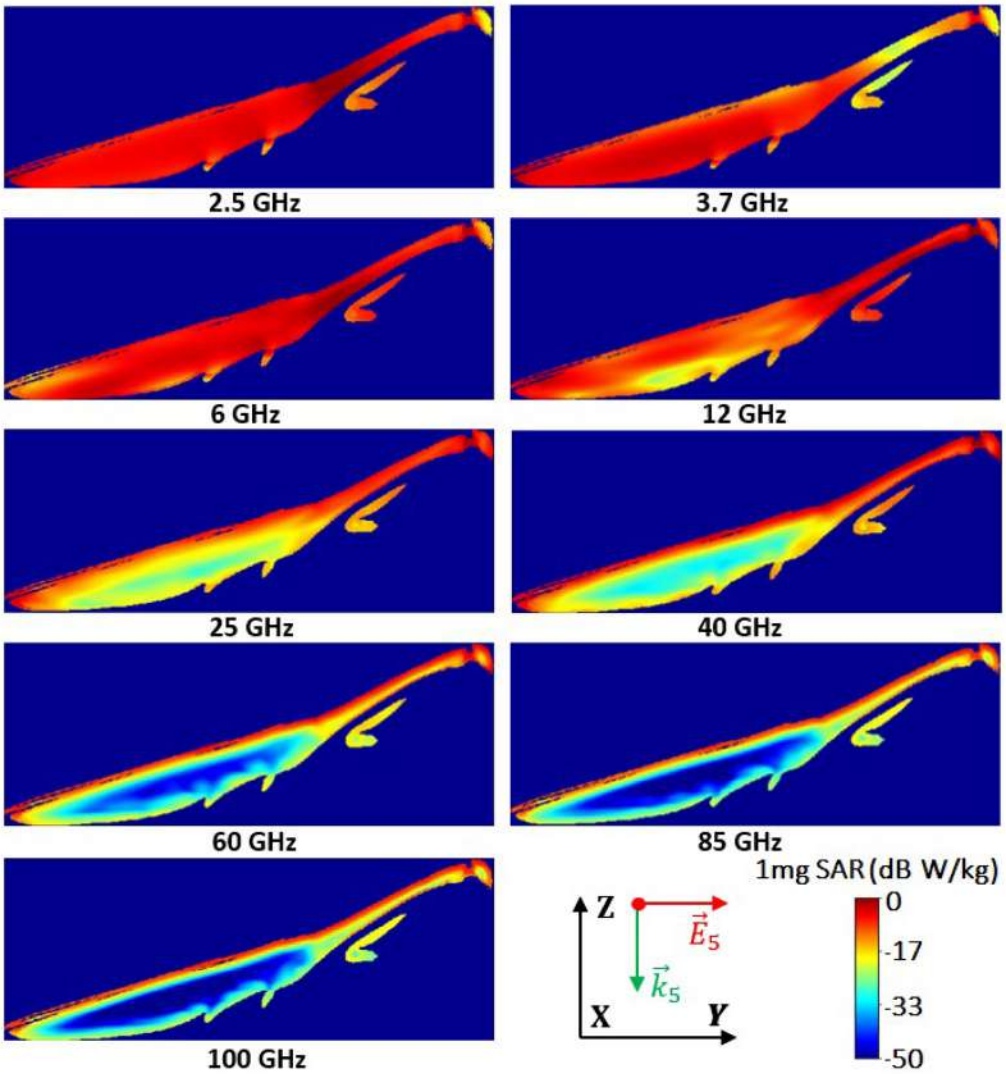


Figure 11. 1 mg SAR distribution inside the mantis model at the parallel section of the ZY plane. The E-vector is directed along the Y-axis (Pol. E5). 1 mg SAR values on the ruler are given in W/kg using a logarithmic (dB) scale.

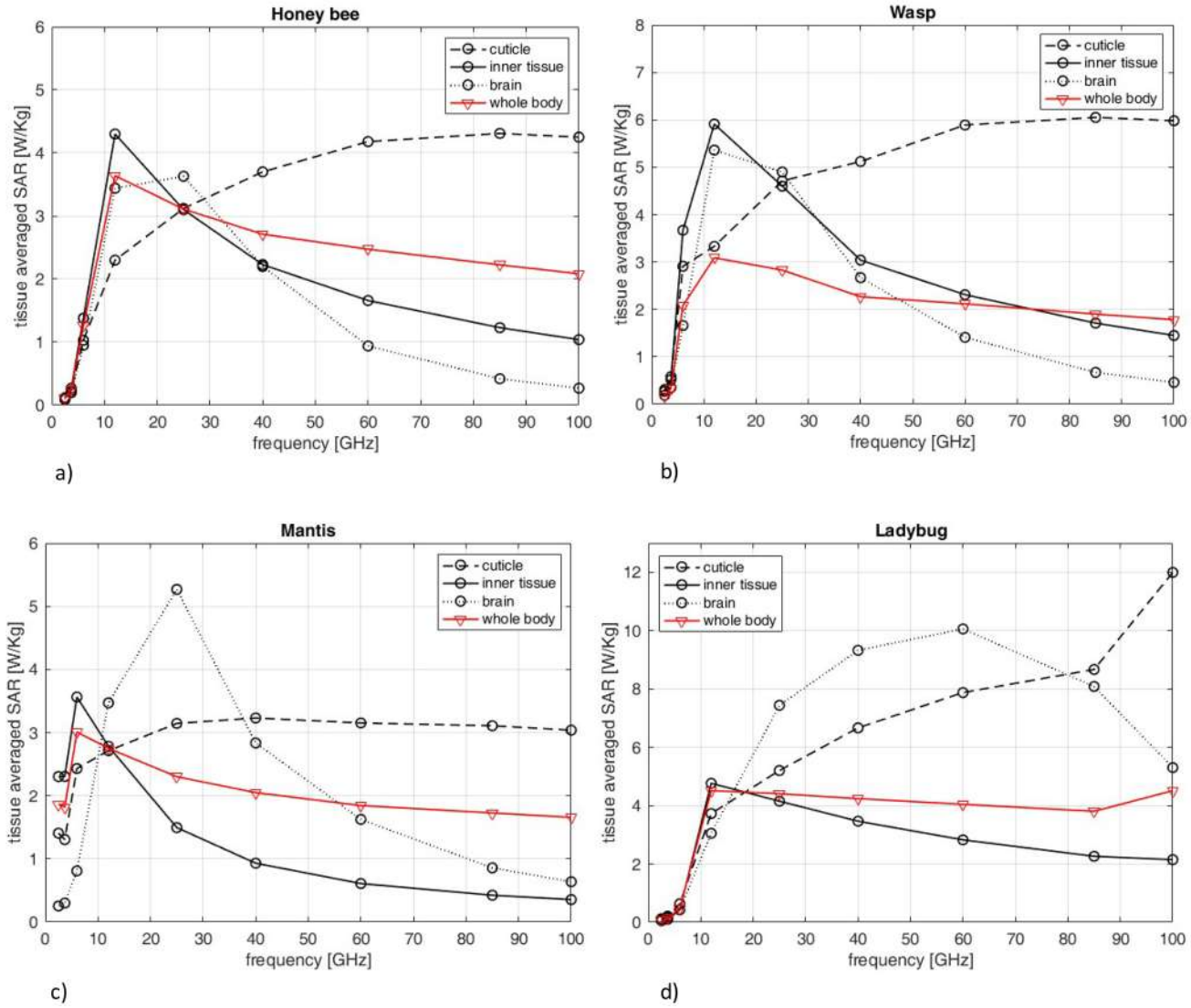


Figure 12. Tissue-averaged SAR values for all tissues and WBA SAR of insects (a) honeybee, (b) wasp, (c) mantis, and (d) ladybug. SAR values averaged for all 10 polarizations of incident E-field for an incident power density of 1 mW/cm^2.

Table 3. Tissue-averaged SAR and WBA SAR values for the 3-tissue sphere with the different tissue properties and with the same tissue properties.

	Cuticle SAR (W/kg)			Inner tissue SAR (W/kg)			Brain SAR (W/kg)			WBA SAR (W/kg)		
	Homog	3 tissue	Diff (%)	Homog	3 tissue	Diff (%)	Homog	3 tissue	Diff (%)	Homog	3 tissue	Diff (%)
2 GHz	0.07	0.07	0.00	0.05	0.05	0.00	0.067	0.068	1.15	0.09	0.09	0.00
3 GHz	0.28	0.32	−12.50	0.26	0.30	−13.33	0.278	0.329	15.50	0.44	0.51	−13.73
6 GHz	1.04	0.99	5.05	1.68	1.64	2.44	1.036	0.993	4.33	1.20	1.05	14.29
12 GHz	2.12	1.83	15.85	1.57	1.51	3.97	2.103	1.854	13.43	2.06	1.84	11.96
25 GHz	3.81	3.32	14.76	1.18	1.17	0.85	3.661	3.139	16.63	1.27	1.15	10.43
60 GHz	6.34	5.7	11.23	0.64	0.75	−14.67	6.349	5.698	11.43	0.49	0.48	2.08

The SAR values are given in W/kg normalized to the incident power density of 1 mW/cm^2.

Table 5 compares the tissue-averaged SAR, 1 mg SAR, and WBA SAR values in W/kg for the same 3-tissue sphere (Figure 4), which were calculated using permittivities and conductivities from Table 1 (used in our EM simulations) and their variations. ε_c = 14.3, ε_i = 25.3, ε_b = 20.2 and σ_c = 18.8 S/m, σ_i = 30.1 S/m, σ_b = 23.7 S/m are the permittivities and conductivities of the cuticle, inner tissue, and brain at 25 GHz (Table 1). The results show that if we increase each permittivity value by 4 and 8 and each conductivity value by 4 and 8 [S/m], the SAR values will decrease, except brain SAR, and the relative differences vary between 2–20%. The SAR values will increase if we reduce the permittivities by 8 and conductivities by 8 S/m; the differences also vary from 2 to 20%. If we increase the permittivities by 4 and decrease the conductivities by 4 S/m, the cuticle and inner tissue SARs will increase, and the brain SAR and 1 mg SAR will decrease and the WBA SAR will be the same.

Table 6 compares the tissue-averaged SAR and WBA SAR values for the smallest insect, the ladybug, for all E-field polarizations at the highest studied frequency (100 GHz)

Table 4. Comparison of the tissue-averaged SAR, 1 mg SAR and WBA SAR values for the 3-tissue sphere with different densities at 60 GHz.

		Cuticle SAR (W/kg)	Inner tissue SAR (W/kg)	Brain SAR (W/kg)	1 mg SAR (W/kg)	WBA SAR (W/kg)
1	ρ_c, ρ_i, ρ_b	5.70	0.79	0.27	6.90	1.37
	ρ_c+50 kg/m^3, ρ_i+50 kg/m^3, ρ_b+50 kg/m^3	5.45	0.75	0.25	6.67	1.31
	Difference %	4.54	4.70	4.80	3.48	4.68
2	ρ_c, ρ_i, ρ_b	5.70	0.79	0.27	6.90	1.37
	ρ_c+100 kg/m^3, ρ_i+100 kg/m^3, ρ_b+100 kg/m^3	5.22	0.72	0.24	6.47	1.25
	Difference %	9.09	9.41	9.61	6.62	9.42
3	ρ_c, ρ_i, ρ_b	5.70	0.79	0.27	6.90	1.37
	ρ_c+150 kg/m^3, ρ_i+150 kg/m^3, ρ_b+150 kg/m^3	5.01	0.69	0.23	6.30	1.20
	Difference %	13.64	14.12	14.39	9.55	14.11
4	ρ_c, ρ_i, ρ_b	5.70	0.79	0.27	6.90	1.37
	ρ_c+200 kg/m^3, ρ_i+200 kg/m^3, ρ_b+200 kg/m^3	4.82	0.66	0.22	6.14	1.15
	Difference %	18.17	18.83	19.17	12.29	18.74
5	ρ_c, ρ_i, ρ_b	5.70	0.79	0.27	6.90	1.37
	ρ_c+100 kg/m^3, ρ_i, ρ_b	5.22	0.79	0.27	6.78	1.35
	Difference %	9.20	0.00	0.00	1.77	1.48
6	ρ_c, ρ_i, ρ_b	5.70	0.79	0.27	6.90	1.37
	ρ_c+200 kg/m^3, ρ_i, ρ_b	4.82	0.79	0.27	6.69	1.34
	Difference %	18.26	0.00	0.00	3.14	2.24

The SAR values are given in W/kg and normalized to the incident power density of 1 mW/cm^2.

Table 5. Comparison of the tissue-averaged SAR, 1 mg SAR and WBA SAR values for the 3-tissue sphere with different permittivities and conductivities at 25 GHz.

		Cuticle SAR (W/kg)	Inner Tissue SAR (W/kg)	Brain SAR (W/kg)	1 mg SAR (W/kg)	WBA SAR (W/kg)
1	ε_c, ε_i, ε_b, σ_c, σ_i, σ_b	1.14	1.16	3.14	4.91	1.4
	ε_c+4, ε_i+4, ε_b+4, σ_c +4 s/m, σ_i+4 s/m, σ_b+4 s/m	1.01	1.07	3.25	4.79	1.33
	Difference %	12.87	8.41	−3.38	2.51	5.26
2	ε_c, ε_i, ε_b, σ_c, σ_i, σ_b	1.14	1.16	3.14	4.91	1.4
	ε_c +4, ε_i+4, ε_b+4, σ_c −4 s/m, σ_i-4 s/m, σ_b-4 s/m	1.42	1.26	2.61	4.63	1.41
	Difference %	−19.72	−7.94	20.31	6.05	−0.71
3	ε_c, ε_i, ε_b, σ_c, σ_i, σ_b	1.14	1.16	3.14	4.91	1.4
	ε_c+8, ε_i+8, ε_b+8, σ_c+8 s/m, σ_i+8 s/m, σ_b+8 s/m	0.95	1.04	3.33	4.68	1.28
	Difference %	20.00	11.54	−5.71	4.91	9.37
4	ε_c, ε_i, ε_b, σ_c, σ_i, σ_b	1.14	1.16	3.14	4.91	1.4
	ε_c −8, ε_i-8, ε_b-8, σ_c −8 s/m, σ_i-8 s/m, σ_b-8 s/m	1.421	1.375	2.864	5.089	1.552
	Difference %	−19.77	−15.64	9.64	−3.52	−9.79
5	ε_c, ε_i, ε_b, σ_c, σ_i, σ_b	1.14	1.16	3.14	4.91	1.4
	ε_c, ε_i+8, ε_b+8, σ_c, σ_i+8 s/m, σ_b+8 s/m	0.99	1.104	2.8	4.78	1.31
	Difference %	15.15	5.07	12.14	2.72	6.87
6	ε_c, ε_i, ε_b, σ_c, σ_i, σ_b	1.14	1.16	3.14	4.91	1.4
	ε_c, ε_i-8, ε_b-8, σ_c, σ_i-8 s/m, σ_b-8 s/m	1.28	1.23	3.68	5.12	1.52
	Difference %	−10.94	−5.69	−14.67	−4.1	−7.89

The SAR values are given in W/kg and normalized to the incident power density of 1 mW/cm^2.

calculated using grid steps of 25 µm and 50 µm. The obtained results show that the differences between the cuticle SAR values are 2–8%, for the inner tissue SARs – 3–13%, for the brain SARs – 4–14%, and for the WBA SARs – 3–10%. Also, the comparison of visualizations of SAR distribution didn't show the displacements of the local maximums of SARs. We have considered 5 directions (top, bottom, front, back, and left) of plane wave direct incidence and 10 polarizations (incidence from the left and right sides are equivalent because of the symmetry of models and we chose one). A small drawback of this study is the fact that we did not consider plane wave incidence at an oblique angle while in reality, the EM waves fall on biological objects from all sides at different angles. It should be noted that it is impossible to consider all possible options due to their abundance.

Since the EM simulation software FDTDLab, which we used for our simulations, is not well-known and widely used software, we have presented its comparison to the well-known EM simulation platform Sim4Life (ZMT, Zurich, Switzerland) to validate our results. Table 7 shows tissue-specific SAR values for a 5 mm radius sphere with muscle tissue calculated by FDTDLab and Sim4Life, and the relative difference (%) between them. The relative difference between the FDTDLab and Si4Life-based values is in the range of 0.9–10% from 2.5 GHz to 40 GHz; at higher frequencies, the difference is in the range of 10–15%. The best agreement between the values was obtained at 2.5, 6, and 12 GHz frequencies when the relative differences don't exceed 4%.

Discussion

Our results show that absorbed SAR values for the honeybee and wasp significantly depend on the incident E-field polarization at frequencies up to 40 GHz. Other papers (Thielens et al. 2018, 2020; De Borre et al. 2021; Herssens et al. 2022; Toribio et al. 2022) have also reported EMF absorption in different insects using different polarizations and showed that differences exist. Our results are thus in line with the literature.

The dimensions of the created honeybee and wasp models are less than the wavelengths for the considered frequencies up to 25 GHz. At the same time, the dimensions of the wasp model are slightly larger than the honeybee model, and the wasp has a longer petiole and more curly surface.

Table 6. Comparison of the tissue-averaged SAR and WBA SAR values for the ladybug using different grid steps at 100 GHz.

	Cuticle SAR (W/kg)			Inner Tissue SAR (W/kg)			Brain SAR (W/kg)			WBA SAR (W/kg)		
	25 µm	50 µm	Diff %	25 µm	50 µm	Diff %	25 µm	50 µm	Diff %	25 µm	50 µm	Diff %
Pol. E1	7.76	7.23	7.33	1.61	1.43	12.59	12.58	11.18	12.52	3.09	2.83	9.19
Pol. E2	8.55	8.23	3.89	2.08	1.88	10.64	12.03	11.48	4.79	3.64	3.41	6.74
Pol. E3	8.26	7.92	4.29	1.94	1.75	10.86	7.50	6.75	11.11	3.46	3.24	6.79
Pol. E4	9.46	9.16	3.28	2.50	2.27	10.13	9.78	9.01	8.55	4.17	3.93	6.11
Pol. E5	9.46	9.13	3.61	2.74	2.48	10.48	5.56	5.11	8.81	4.35	4.08	6.62
Pol. E6	9.33	8.95	4.25	2.76	2.52	9.52	2.95	2.64	11.83	4.34	4.07	6.65
Pol. E7	12.92	12.19	5.99	1.77	1.69	4.73	0.98	0.94	4.26	4.45	4.21	5.70
Pol. E8	13.21	12.27	7.66	1.82	1.75	4.00	1.10	0.97	13.40	4.55	4.27	6.56
Pol. E9	22.28	20.96	6.30	2.68	2.60	3.08	2.54	2.24	13.39	7.37	7.01	5.14
Pol. E10	24.58	23.90	2.85	3.28	3.10	5.81	2.91	2.73	6.59	8.39	8.09	3.71

The SAR values are given in W/kg and normalized to the incident power density of 1 mW/cm^2.

Table 7. Comparison of the tissue-averaged SAR values for a muscled sphere (r = 5 mm) calculated by Sim4Life and FDTDLab, and the relative difference (%) between them for the frequencies from 2.5 to 100 GHz.

	Sim4Life muscle SAR (W/kg)	FDTDLab muscle SAR (W/kg)	Difference (%)
2.5 GHz	0.12	0.12	0.00
3.7 GHz	1.48	1.57	−5.73
6 GHz	1.55	1.50	3.33
12 GHz	1.46	1.45	0.69
25 GHz	1.28	1.18	8.47
40 GHz	1.20	1.10	9.09
60 GHz	1.17	1.06	10.38
85 GHz	1.13	1.01	11.88
100 GHz	1.10	0.96	14.58

SAR values are normalized to the incident power density of 1 mW/cm^2.

Based on the obtained results from Figure 8(a), a sharp variation of the SAR values depending on the polarization up to 40 GHz frequencies and higher SAR values for wasp (Figure 8(b)) compared to honeybee and their localizations can be caused by the insects' body peculiarities and also by the difference in body sizes.

In this study, we used insect models processed using graphics software. Future validation of the obtained results could be obtained by conducting EM simulations using insect models created by Micro-CT Imaging, as the insect models obtained in this way are closer to reality.

Figure 12(a-d) shows that the tissue-specific SAR values depend on frequency for all insects. Cuticle SARs increase with increasing frequency. At lower frequencies, especially at 6 and 12 GHz, the inner tissue SARs are greater than cuticle SARs for all insects and then decrease with increasing frequency up to 100 GHz because the EMF penetration depth decreases at high frequencies. Maximal tissue-averaged brain SARs greater than the ones found in the cuticle and inner tissue SARs are observed at 12 and 25 GHz frequencies for honeybee, wasp and mantis, and for the ladybug at 25, 40, 60, and 85 GHz.

In the presented research, we have averaged SAR values over a volume of 1 milligram of tissue. Such an averaging of SAR values for small-sized insects with a mass close to 1 gram (ladybug, honeybee, and wasp) was introduced for the first time. It was impossible to average SAR in accordance with international standards over a volume of 1 g and 10 g of tissues. 1 mg SAR values are more informative and could be considered as a standard in the future for small-sized biological organisms, like insects, if it could be demonstrated that this quantity can be seen as a proxy for biological effects associated with RF-EMF exposure in a certain frequency range. Future studies should be aimed at determining such a relationship. Finally, we studied the influence of the choice of simulation parameters and settings on the obtained results.

In our future studies, we plan to investigate different SAR averaging masses to harmonize RF-EMF safety and compliance doses and develop recommendations about RF-EMFs' safe doses concerning insects and other small-sized organisms. To achieve this goal and select the best-averaging mass of SAR, our studies consider evaluating SAR with different averaging masses, such as 10 mg, 5 mg, 1 mg, 0.5 mg, and 0.1 mg, and conducting thermal simulations to determine the correlation between the SAR and temperature increase distributions.

The temperature increase in insect tissues that will be caused by the EMF absorption of the fields might seem small because insects are capable of tolerating a broad range of environmental temperatures, up to 40–50 °C (Heinrich 1981). However, it is crucial to recognize that tolerance does not equate to the absence of significant effects from temperature variations, as insects are ectothermic organisms, meaning their physiological processes are heavily influenced by ambient temperatures. Numerous studies have demonstrated that even minor temperature changes can lead to profound behavioral and developmental consequences in various insect species, including drosophila, mosquitoes and bees (Tautz et al. 2003; Christiansen-Jucht et al. 2014; Classen et al. 2015; Evans et al. 2018; Winkler et al. 2020; Klepsatel and Gáliková 2022).

Conclusion

The paper presented a study of RF-EMF dosimetry of honeybee worker, wasp, mantis, and ladybug from 2.5 to 100 GHz, including frequencies that will be utilized in future 5 G technologies.

Discrete, 3-tissue heterogenous insect 3D models were created and used for FDTD modeling.

The whole-body averaged SAR values and tissue-averaged SAR values were estimated in insects' tissues for 9 considered frequencies and 10 polarizations of incident plane wave. For the first time, 1 mg SAR values were determined in insect tissues.

The obtained results showed SAR values in honeybee, wasp, ladybug, and mantis body tissues, which depend on

the direction of the incident plane wave and polarization, frequency, and the insects' body sizes and peculiarities.

The highest values of the peak 1 mg SAR for the honeybee and wasp – 39.2 W/kg and 169.2 W/kg for an incident field strength of 1 mW/cm^2, were observed when E-field polarization was directed along the insect's length (pol. E3, E5, E9).

The obtained results showed maximal tissue-specific SAR values in the brain at 25 GHz for the honeybee (3.6 W/kg), 12 GHz for the wasp (5.4 W/kg), 25 GHz for the mantis (5.2 W/kg), and 60 GHz for the ladybug (10 W/kg), all for an incident power density of 1 mW/cm^2. Maximal EMF absorption in the inner tissue was observed at 12 GHz, 4.3 W/kg, 5.9 W/kg, 4.8 W/kg for the honey bee, waps, and ladybud, respectively, and for the mantis 3.3 W/kg at 6 GHz for an incident power density of 1 mW/cm^2. The absorption in insects' cuticles increased proportionally with frequency. For example, for the ladybug, the tissue-specific SAR in the cuticle was 0.1 W/kg at 2.5 Ghz and 11.9 W/kg at 100 GHz for the same incident power density of 1 mW/cm^2.

Future studies will consider introducing insect models that will be obtained using micro-CT scanning, examining the effects of high-frequency electromagnetic fields on other insects of different forms and sizes, conducting thermal simulations along with EM simulations, and evaluating temperature rise in insect tissues.

Based on the present results, we expect this research to have an impact on (environmental) policymaking and standardization and regulation regarding RF-EMF emissions. We expect to contribute to the harmonization of 5 G EMF safety and compliance doses and to the development of future recommendations about safe frequencies and doses of 5 G-EMF on the organisms studied in the present research.

Acknowledgments

We are grateful to Prof. Henry Lai for providing feedback on the manuscript.

Disclosure statement

No potential conflict of interest was reported by the author(s).

Funding

The research was supported by the Shota Rustaveli National Science Foundation of Georgia's grant (fellowship) for Young Scientists (#YS-21-109).

Notes on contributors

Vera Jeladze, PhD, is a Senior Research Fellow at the Institute of Cybernetics of Georgian Technical University, Department of Biocybernetics, and a Professor at the Georgian National University SEU, Department of Information Technology, Tbilisi, Georgia.

Tamar Nozadze, PhD, is an Assistant Professor at the Department of Electric and Electronic Engineering, Tbilisi State University, Tbilisi, Georgia.

Besarion Partsvania, PhD, is Chief Research Fellow and Head of the Department of Biocybernetics, Institute of Cybernetics of Georgian Technical University, Tbilisi, Georgia.

Arno Thielens, PhD, is a research associate professor and the director of the RF and mm-wave facility of the Graduate Center of the City University of New York, Photonics Initiative, ASRC, New York, USA.

Levan Shoshiashvili, PhD, is an Assistant Professor at the Department of Electric and Electronic Engineering, Tbilisi State University, Tbilisi, Georgia.

Teimuraz Gogoladze, PhD, is a Research Fellow at the Institute of Cybernetics of Georgian Technical University, Department of Biocybernetics.

ORCID

Vera Jeladze http://orcid.org/0000-0003-2264-8935
Tamar Nozadze http://orcid.org/0000-0001-7861-1264
Besarion Partsvania http://orcid.org/0009-0006-0946-2238
Arno Thielens http://orcid.org/0000-0002-8089-6382

References

Aslan CE, Liang CT, Galindo B, Kimberly H, Topete W. 2016. The role of honey bees as pollinators in natural areas. Nat Areas J. 36(4):478–488. doi:10.3375/043.036.0413.

Balmori A. 2015. Anthropogenic radiofrequency electromagnetic fields as an emerging threat to wildlife orientation. Sci Total Environ. 518-519:58–60. doi:10.1016/j.scitotenv.2015.02.077.

CadNav 3D. 2024. [accessed 2024 Apr 28]. https://www.cadnav.com/.

Cammaerts MC, Vandenbosch GAE, Volski V. 2014. Effect of short-term GSM radiation at representative levels in society on a biological model: the ant *Myrmica sabuleti*. J Insect Behav. 27(4):514–526. doi:10.1007/s10905-014-9446-4.

Christiansen-Jucht C, Parham PE, Saddler A, Koella JC, Basáñez MG. 2014. Temperature during larval development and adult maintenance influences the survival of *Anopheles gambiae* s.s. Parasites Vectors. 7(1):489. doi:10.1186/s13071-014-0489-3.

Classen A, Peters MK, Kindeketa WJ, Appelhans T, Eardley CD, Gikungu MW, Hemp A, Nauss T, Steffan-Dewenter I. 2015. Temperature versus resource constraints: which factors determine bee diversity on Mount Kilimanjaro, Tanzania? Global Ecol Biogeogr. 24(6):642–652. doi:10.1111/geb.12286.

Colombi D, Thors B, Tornevik C. 2015. Implications of EMF exposure limits on output power levels for 5 G devices above 6 Ghz. IEEE Antennas Wirel Propag Lett. 14:1247–1249. doi:10.1109/LAWP.2015.2400331.

De Borre E, Joseph W, Aminzadeh R, Müller P, Boone MN, Josipovic I, Hashemizadeh S, Kuster N, Kühn S, Thielens A. 2021. Radio-frequency exposure of the yellow fever mosquito (*A. aegypti*) from 2 to 240 GHz. PLoS Comput Biol. 17(10):e1009460. doi:10.1371/journal.pcbi.1009460.

Dixon AFG. 2000. Insect predator-prey dynamics: ladybird beetles and biological control. New York (NY): Cambridge University Press.

Evans RK, Toews MD, Sial AA. 2018. Impact of short- and long-term heat stress on reproductive potential of *Drosophila suzukii* Matsumura (Diptera: Drosophilidae). J Therm Biol. 78:92–99. doi:10.1016/j.jtherbio.2018.09.011.

Fauzi A, Corebina AD. 2015. The effect of EMF radiation emitted by mobile phone to insect population using *Drosophila melanogaster* as a model organism. In Proceedings of the 6th International Conference on Global Resource Conservation (ICGRC); Nov 30–Dec 2; Malang (EJ), Indonesia. p. 16–20.

Hand JW. 2008. Modelling the interaction of electromagnetic fields (10 MHz–10 GHz) with the human body: methods and applications. Phys Med Biol. 53(16):R243–286. doi:10.1088/0031-9155/53/16/R01.

Hasgall PA, Di Gennaro F, Baumgartner C, Neufeld E, Lloyd B, Gosselin MC, Payne D, Klingenböck A, Kuster N. 2022. IT'IS data-

base for thermal and electromagnetic parameters of biological tissues. Version 4.1. doi:10.13099/VIP21000-04-1. itis.swiss/database
Heinrich B. 1981. Insect thermoregulation. New York: Wiley.
Heinze S, El Jundi B, Berg BG, Homberg U, Menzel R, Pfeiffer K, Hensgen R, Zittrell F, Dacke M, Warrant E, et al. 2021. A unified platform to manage, share, and archive morphological and functional data in insect. neuroscience. Elife. 10:e65376. doi:10.7554/eLife.65376.
Herssens H, Toribio D, De Borre E, Thielens A. 2022. Whole-body averaged absorbed power in insects exposed to far-field radio-frequency electromagnetic fields. IEEE Trans Antennas Propagat. 70(11):11070–11078. doi:10.1109/TAP.2022.3209201.
Hirata A, Kodera S, Wang J, Fujiwara O. 2007. Dominant factors influencing whole-body average SAR due to far-field exposure in whole-body resonance frequency and GHz regions. Bioelectromagnetics. 28(6):484–487. doi:10.1002/bem.20335.
International Commission on Non-Ionizing Radiation Protection. 2020. Guidelines for limiting exposure to electromagnetic fields (100 KHz to 300 GHz). Health Phys. 118(5):483–524. doi:10.1097/HP.0000000000001210.
Klepsatel P, Gáliková M. 2022. Developmental temperature affects thermal dependence of locomotor activity in Drosophila. J Therm Biol. 103:103153. doi:10.1016/j.jtherbio.2021.103153.
Lázaro A, Chroni A, Tscheulin T, Devalez J, Matsoukas C, Petanidou T. 2016. Electromagnetic radiation of mobile telecommunication antennas affects the abundance and composition of wild pollinators. J Insect Conserv. 20(2):315–324. doi:10.1007/s10841-016-9868-8.
Liorni I, Capstick M, van Wel L, Wiart J, Joseph W, Cardis E, Guxens M, Vermeulen R, Thielens A. 2020. Evaluation of specific absorption rate in the far-field, near-to-far field and near-field regions for integrative radiofrequency exposure assessment. Radiat Prot Dosimetry. 190(4):459–472. doi:10.1093/rpd/ncaa127.
Marec F, Ondrácek J, Brunnhofer V. 1985. The effect of repeated microwave irradiation on the frequency of sex-linked recessive lethal mutations in *Drosophila melanogaster*. Mutat Res. 157(2-3):163–167. doi:10.1016/0165-1218(85)90112-0.
Ollerton J, Winfree R, Tarrant S. 2011. How many flowering plants are pollinated by animals? OIKOS. 120(3):321–326. doi:10.1111/j1600-0706.201018644x.
Open3DModel. 2024. [accessed 2024 Apr 28]. https://open3dmodel.com/.
Pall ML. 2013. Electromagnetic fields act via activation of voltage-gated calcium channels to produce beneficial or adverse effects. J Cell Mol Med. 17(8):958–965. doi:10.1111/jcmm.12088.
Papa G, Maier R, Durazzo A, Lucarini M, Karabagias IK, Plutino M, Bianchetto E, Aromolo R, Pignatti G, Ambrogio A, et al. 2022. The honey bee *Apis mellifera*: an insect at the interface between human and ecosystem health. Biology (Basel). 11(2):233. doi:10.3390/biology11020233.
Pi A, Khan F. 2011. An introduction to millimeter-wave mobile broadband systems. IEEE Commun Mag. 49(6):101–107. doi:10.1109/MCOM.2011.5783993.
Prezoto F, Maciel TT, Detoni M, Mayorquin AZ, Barbosa BC. 2019. Pest control potential of social wasps in small farms and urban gardens. Insects. 10(7):192. doi:10.3390/insects10070192.
Rosner R, von Hadeln J, Salden T, Homberg U. 2017. Anatomy of the lobula complex in the brain of the praying mantis compared to the lobula complexes of the locust and cockroach. J Comp Neurol. 525(10):2343–2357. doi:10.1002/cne.24208.
Sanborn A. 2008. Thermoregulation in insects. In Encyclopedia of Entomology. 2nd ed. Dordrecht: Springer. p. 3757–3760.
Schuster MF, Whicker AD. 1983. The European praying mantis (*Mantis religiosa* L.) as a predator of the red-legged grasshopper (*Melanoplus femurrubrum* (De Geer)). Environmental Entomology. 12(4):1008–1012.
Taflove A, Hagness SC. 2005. Computational electrodynamics: the finite-difference time-domain method. 3rd ed. Norwood: Artech House.
Tautz J, Maier S, Groh C, Rossler W, Brockmann A. 2003. Behavioral performance in adult honey bees is influenced by the temperature experienced during their pupal development. Proc Natl Acad Sci U S A. 100(12):7343–7347. doi:10.1073/pnas.1232346100.
Thielens A, Bell D, Mortimore DB, Greco MK, Martens L, Joseph W. 2018. Exposure of insects to radio-frequency electromagnetic fields from 2 to 120 GHz. Sci Rep. 8(1):3924. doi:10.1038/s41598-018-22271-3.
Thielens A, Greco MK, Verloock L, Martens L, Joseph W. 2020. Radio-frequency electromagnetic field exposure of western honey bees. Sci Rep. 10(1):461. doi:10.1038/s41598-019-56948-0.
Toribio D, Joseph W, Thielens A. 2022. Near field radio-frequency electromagnetic field exposure of a western honey bee. IEEE Trans Antennas Propagat. 70(2):1320–1327. doi:10.1109/TAP.2021.3111286.
Vijver MG, Bolte JF, Evans TR, Tamis WL, Peijnenburg WJ, Musters CJ, de Snoo GR. 2014. Investigating short-term exposure to electromagnetic fields on reproductive capacity of invertebrates in the field situation. Electromagn Biol Med. 33(1):21–28. doi:10.3109/15368378.2013.783846.
Wang S, Tang J. 2001. Radio frequency and microwave alternative treatments for nut insect control: a review. Int Agric Eng J. 10(3–4):105–120.
Winkler A, Jung J, Kleinhenz B, Racca P. 2020. A review on temperature and humidity effects on Drosophila *suzukii* population dynamics. Agriculture and Forest Entomology. 22(3):213–222.
Yee K. 1966. Numerical solution of initial boundary value problems involving Maxwell's equations in isotropic media. IEEE Trans Antennas Propag. 14(3):302–307.